JOURNAL OF AIRCRAFT
Vol. 35, No. 6, November–December 1998

Flowfield and Acoustic Measurements from a Model Tiltrotor in Hover

David R. Polak*
United Technologies Research Center, East Hartford, Connecticut 06108-1127
and
Albert R. George†
Cornell University, Ithaca, New York 14853-7501

Rotor inflow aerodynamics and noise measurements were made on three configurations of an 8% scale model of the XV-15 tiltrotor in hover: 1) single isolated rotor, 2) two rotors with no fuselage, and 3) complete tiltrotor aircraft. For the tiltrotor aircraft configuration and for the configuration of two rotors without the fuselage, the mean inflow velocity was higher at $\psi = 270$ deg compared with the rest of the rotor disk, leading to reduced blade angle of attack and blade loading in this region. This azimuthally varying blade loading caused an impulsive noise that radiated preferentially behind the model. For the complete tiltrotor configuration, the turbulence ingested by the rotors was intermittent and depended on the instantaneous position of the fountain flow, which shifted from side to side across the longitudinal plane of the model. The fountain turbulence had a higher velocity scale, smaller length scale, and was closer to isotropic than the ingested ambient turbulence. The tiltrotor configuration radiated less harmonic noise, but more broadband noise than the configuration with two rotors and no fuselage. Diagonal fences on the wings of the tiltrotor reduced the inflow turbulence intensity in the fountain region by a factor of about 3, and reduced the noise by 4.1 dBA behind the model. Scaling relations were derived to extrapolate the model measurements to the full-scale XV-15.

Nomenclature

A_{blade} = rotor blade planform area, m^2
b = number of rotor blades
C = wing chord, m
c_{tip} = rotor blade tip chord, m
$E(\kappa)$ = three-dimensional energy spectrum, m^3/s^2
$F_{11}(\kappa_1)$ = one-dimensional spectrum of u_s, m^3/s^2
$F_{22}(\kappa_1)$ = one-dimensional spectrum of u_n, m^3/s^2
f = frequency, Hz
h = rotor disk-to-wing clearance, m
ℓ = turbulence length scale, m
M_{tip} = tip Mach number
p = acoustic pressure, Pa
R = rotor radius, m
Re_{in} = inflow Reynolds number, $2wC/\nu$
Re_ℓ = turbulence Reynolds number, $u\ell/\nu$
Re_{tip} = tip Reynolds number, $V_{\text{tip}}c_{\text{tip}}/\nu$
r = radial coordinate, m
ρ = source-observer propagation distance, m
s = wake spacing, w/f_{bp}, m
t = time, s
$\langle U \rangle$ = mean velocity, m/s
u = turbulence velocity scale, m/s
u_b = binormal fluctuating velocity component, m/s
u_n = normal fluctuating velocity component, m/s
u_s = streamwise fluctuating velocity component, m/s
V_{tip} = blade tip speed, ΩR, m/s
w = mean induced hover velocity, m/s
z = axial coordinate, positive above rotor plane, m
η = Kolmogorov microscale, m
κ = wave number, m^{-1}
ν = kinematic viscosity, m^2/s
σ = solidity of each rotor, $bA_{\text{blade}}/\pi R^2$
ψ = azimuthal coordinate, positive in direction of rotation, deg
Ω = rotor angular speed, rad/s

Subscripts
bp = blade passage
f = full scale
m = model scale
th = theoretical
z = axial direction
1 = streamwise direction

Received April 20, 1996; revision received July 7, 1998; accepted for publication on July 9, 1998.

*Associate Research Engineer, 411 Silver Lane. Member AIAA.
†J. F. Carr Professor of Mechanical Engineering. Associate Fellow AIAA.

Introduction

BECAUSE of their speed, range, fuel economy, and efficient use of vertiport area, tiltrotor aircraft are good candidates for short- to medium-range civil transport.[1] However, to be successfully integrated into civilian airspace, especially near city centers, it is important to keep the tiltrotor's noise levels acceptable to the public.[2] Before noise-reduction strategies can be fully developed, tiltrotor noise sources must be understood, modeled, and accurately predicted.

While a tiltrotor hovers, the close proximity of the two rotors, main wings, and fuselage creates complex rotor–rotor and rotor–airframe aerodynamic interactions. For example, the wing and fuselage provide a partial ground plane that causes the rotor downwash to flow toward the aircraft's longitudinal plane of symmetry, where the opposing flows collide, producing a highly turbulent, unsteady fountain flow with an upward velocity component. McVeigh[3] sketched and described this flow, whereas George et al.[4] developed a model for it based on flow visualization and inviscid computational fluid dynamics (CFD) calculations. More sophisticated calculations of tiltrotor hover interference flows have also been reported.[5–9] The tiltrotor hover interference flows typically cause a figure of

merit reduction of about 3%, and a download penalty as large as 15% of total rotor thrust.[10–12]

The interaction of the rotors with each other and with the fountain flow causes increased loading noise that is preferentially radiated behind the aircraft because of the direction of rotation of the rotors (from wing leading edge to trailing edge as they sweep over the main wings). Lee and Mosher[13] first identified hover mode as a noise problem for tiltrotors. George et al.[4] reviewed tiltrotor noise mechanisms, and performed broadband and discrete acoustic calculations of XV-15 hover noise. The predictions were later improved upon[14–17] and compared with the full-scale XV-15 hover data of Conner and Wellman.[18] Further noise calculations were presented by Tadghighi et al.[8] In general, most of the noise calculations show good agreement with experiment in directivity and overall levels. However, the relatively simple fountain-flow models do not capture all of the physical phenomena, particularly the turbulence characteristics and unsteadiness. Some small-scale experiments have revealed the complexity of tiltrotor hover interference flows,[19,20] and highlight the need for more detailed measurements.

Relatively little research has been done to control or reduce tiltrotor hover interference flows. Wood and Peryea[21] were able to reduce the XV-15 download penalty by as much as 3.5%, using flow control devices on the main wings, but similar devices produced little effect in the noise experiments of Mosher and Light.[22]

The purpose of the present research was to improve understanding of tiltrotor hover interference flows and the rotor noise they influence. Experiments were performed on an 8% scale model of the XV-15. Two-component hot-wire anemometry was used to measure mean velocities, streamwise spectra, and one component of cross-stream spectra. Reduction of the measurements yielded three-dimensional energy spectra of the turbulence, along with characteristic scales of length and velocity. Far-field acoustic measurements were also made. To isolate the flow and noise mechanisms, three configurations of the model were investigated: 1) single isolated rotor, 2) two rotors with no fuselage, and 3) complete tiltrotor aircraft. Scaling relations were derived to extrapolate the model measurements to the full-scale XV-15. Finally, the effects of diagonal fences, a device designed to control the rotor–airframe interaction flows, were investigated.

Experimental Apparatus and Procedure

Figure 1 shows the 8% scale model of the XV-15 in hover. Two uncoupled electric motors powered rigid, fixed-pitch, two-bladed rotors at an equivalent full-scale rotor plane altitude of $5.2R$. Each rotor was operated at a thrust coefficient of 0.0078 (compared with about 0.011 for the full scale), and a figure of merit of about 0.63. Rotor speeds were matched with a stroboscope and variable transformers. For the acoustic measurements, photo diodes and a comparator circuit were used to trigger the data-acquisition system only when the rotors were in phase.

The rotor phase was not controlled during the flow visualization or hot-wire experiments. However, some more recent flow visualization, seven-hole pressure probe, and hot-wire experiments on the model have shown that the mean flows being studied were only slightly affected by rotor phase. The details of the turbulent flows were most likely affected by rotor phase (especially under the rotor plane), but evidence shows that most of the tip and wake vorticity was cascaded into the turbulence of the fountain flow, so that few discrete structures existed above the rotor plane. If this was true, then the global time-averaged energy input to the fountain flow was more important then the time-resolved details of how that energy got into the flow.

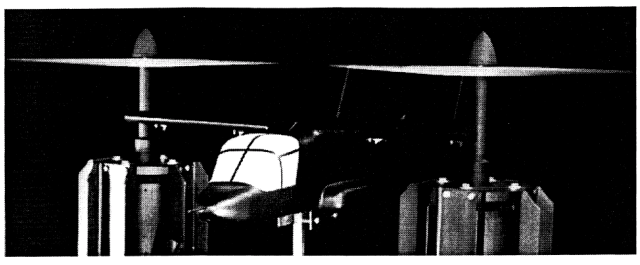

Fig. 1 Eight percent model of the XV-15 tiltrotor in hover.

A flow control device, the diagonal fence, was also tested on the model. The fences intersected the vertical plane through the rotor centerlines at $r/R = 0.85$, at an angle of about 15 deg. The fence geometry was not rigorously optimized, but flow visualization was used to find a configuration that blocked the transport of blade wake and tip vorticity by the mean flow backup between the rotor disks.

Description of the Experiment

Flow visualization was accomplished using neutrally buoyant helium-filled soap bubbles formed by a Sage Action Model 3 Bubble Generator, and 35-mm photography. The bubbles passed through the rotor plane intact, and were illuminated by a high-intensity xenon arc lamp.

A TSI 1240 crossflow X wire, TSI 1052 linearizers, and TSI 1050 constant-temperature anemometers were used for the hot-wire experiments. The equations of Champagne and Sleicher[23] for linearized constant temperature operation were used. The measurements were corrected for ambient temperature and high-turbulence intensity.[24] Ensemble averaging was accomplished with a 12-bit data acquisition board and Macintosh computer, for a typical dynamic range of about 70 dB. Each ensemble was digitized at a rate of 2000 Hz for a duration of 0.5 s (about 29 rotor revolutions). Typically, 1000 ensembles were employed. Experimental uncertainty was estimated using the method of Kline and McClintock[25] (see Ref. 26 for details). A HP 3582A spectrum analyzer was used for the Fourier analysis, with Hann windowing, 256 ensemble averages, and a 6-Hz bandwidth. The dynamic range of the hot-wire spectral analysis was improved by acquiring multiple bandpassed spectra, then merging the measurements. Spectra were measured in the time domain and converted to wave-number space using Taylor's frozen turbulence hypothesis

$$\kappa_1 = 2\pi f/\langle U \rangle \tag{1}$$

The flow visualization and hot-wire measurements were performed indoors. The nearest wall was $9.3R$ away from the center of the model, and the ceiling was $6.8R$ above the rotor plane. On two sides of the model, the rotor downwash could freely travel for at least $13R$ along the laboratory floor. The fourth side of the model was open to a very large two-story loading dock. Although some room recirculation was present, the rotors were not as close to the walls and ceiling as those of Piziali and Felker[27] ($6R$ away from the walls, $4R$ away from the ceiling).

The model acoustic experiments were conducted outdoors during very low wind conditions in an empty, asphalt-surfaced parking lot to approximate a free field. The nearest building was more than 35 m away from the model. The microphone locations were arranged so that sound reflected from the building was computed to be at least 15 dB lower than incident sound, assuming spherical propagation and perfect reflection. A B&K-1/2 in. condenser microphone with a windscreen was used with a Krohn-Hite 4-pole Butterworth bandpass filter (bandpass frequencies set to 0.17 and $67.0f_{bp}$). The filter introduced negligible amplitude distortion in the measurement frequency range, but there was about a 30-deg phase distortion at f_{bp}. Acoustic waveforms were measured using the same Macintosh data acquisition computer used for the turbulence measurements, and spectra were measured using the same Hewlett-Packard spectrum analyzer. The microphone was placed on the

ground at distances of 42, 24, and 16R directly behind and in front of the model, at angles of 7.1, 12.6, and 18.1 deg, respectively, below the rotor plane. Unfortunately, measurements could not be obtained at steeper angles because of wind noise from the rotor downwash. With respect to far-field directivity lobes, observer locations directly in front of or directly behind the model were least affected by the two-bladed model rotors compared with three blades for the full-scale XV-15.[26]

Turbulence Data Reduction

Because there was relative motion between the stationary hot-wire probe and the rotor blades, the measured turbulence spectra contained contributions from the potential flowfield of the rotors, from ambient turbulence, and from the fountain flow (when present). To remove the potential rotor flow fluctuations from the measurements, a narrow bandwidth analysis was used to ensure that the broadband part of the spectra between the discrete rotor blade passing peaks were unaffected by the peaks. Assuming that the turbulence and potential flowfields were uncorrelated, the peaks of the blade-passing frequency were then removed, and the remaining broadband spectra were smoothly interpolated.

For a stationary flow, a model for any velocity component is[28]

$$U_i(t) = \langle U_i \rangle + \sum_{n=1}^{N} A_{ni} \cos(2\pi f_n t + \phi_n) + X_i(t) \tag{2}$$

where $X_i(t)$ is an independent random process representing the turbulent velocity fluctuations, defined so that $\langle X_i \rangle = 0$. The power spectral density of $U_i(t)$ is[28]

$$S_{U_i}(f) = \langle U_i \rangle^2 \delta(f) + \sum_{n=1}^{N} \frac{A_{ni}^2}{2} \delta(f - f_n) + S_{X_i}(f) \tag{3}$$

Thus, the procedure for removing the potential rotor flow fluctuations from the measurements is equivalent to removing the summation terms on the right side of Eq. (3). Filtering the mean velocity, the resulting spectrum becomes

$$S_{U_i}(f) = S_{X_i}(f) \tag{4}$$

which is the desired power spectral density of the turbulent velocity fluctuations.

Assuming axisymmetric turbulence

$$\langle u_n^2 \rangle = \langle u_b^2 \rangle \neq \langle u_s^2 \rangle \tag{5}$$

the three-dimensional energy spectrum of the total energy was computed from the interpolated part of the measured $F_{11}(\kappa_1)$ and $F_{22}(\kappa_1)$[29]

$$E(\kappa) = -\left(\frac{\kappa}{2}\right) \frac{d[F_{11}(\kappa) + 2F_{22}(\kappa)]}{d\kappa} \tag{6}$$

along with the velocity and length scales

$$u^2 = \int_0^{1/\eta} \left[\frac{2E(\kappa)}{3}\right] d\kappa \tag{7}$$

$$\ell = 1/\kappa \quad \text{at peak of} \quad E(\kappa) \tag{8}$$

The Kolmogorov microscale was estimated from[30]

$$\eta = (1.28 \ell \nu^3/u^3)^{1/4} \tag{9}$$

Figure 2 shows an example of a measured one-dimensional spectrum, $F_{11}(\kappa_1)$, and the interpolated broadband part of the spectrum, nondimensionalized by u and ℓ of Eqs. (7) and (8).

Scaling Analysis

Because the measurements were made at model scale, it was necessary to analyze how the experimental results related to the full-scale XV-15. When an experiment is performed at reduced scale, it is usually not possible to hold all of the pertinent dimensionless parameters constant. In these cases, one must determine whether the distortions are important and if corrections can be made for them.

Table 1 lists characteristic scales of length, velocity, and time, along with dimensionless numbers for the model and full-scale XV-15.[31] The scaling relations given in Table 1 were used to extrapolate the model measurements to the full-scale, based on the governing equations and the characteristic scales of the flow.[32] As shown by Polak and George,[32] most of the fountain-flow turbulence is produced by the blade wake, and then transported by the mean flow backup between the rotor disks, so that this turbulence was assumed to have length and velocity scales proportional to R and w, respectively. To estimate the acoustic far-field pressure scaling, linearized aerodynamics and Farassat's formulation 1A[33] for loading noise produced by unsteady force effects were used

$$\frac{p_f}{p_m} = \left(\frac{\sigma_f}{\sigma_m}\right)\left(\frac{b_m}{b_f}\right)\left(\frac{R_f}{R_m}\right)^2\left(\frac{\rho_m}{\rho_f}\right)\left(\frac{1 - M_{\text{tip},m}}{1 - M_{\text{tip},f}}\right)^2\left(\frac{V_{\text{tip},f}}{V_{\text{tip},m}}\right)^2 \times \left(\frac{R_m}{R_f}\right)\left(\frac{w_f}{w_m}\right) \tag{10}$$

Because it was assumed that $u \propto w$, and $\ell \propto R$, Eq. (10) applies equally well for noise caused by azimuthally varying blade loadings or interactions between the rotor and the fountain-flow turbulence.

None of the dimensionless parameters listed in Table 1 for the model and full-scale XV-15 match perfectly. For example, M_{tip} was much lower on the model, but this had little effect on the subsonic fountain flow, and could be approximately accounted for in the acoustic experiments as shown in Eq. (10). Also, Re_{tip} was smaller on the model. To help eliminate any laminar-flow acoustic sources, a 0.06-mm-diam nylon monofilament was cemented along the 5% chord line of the outer

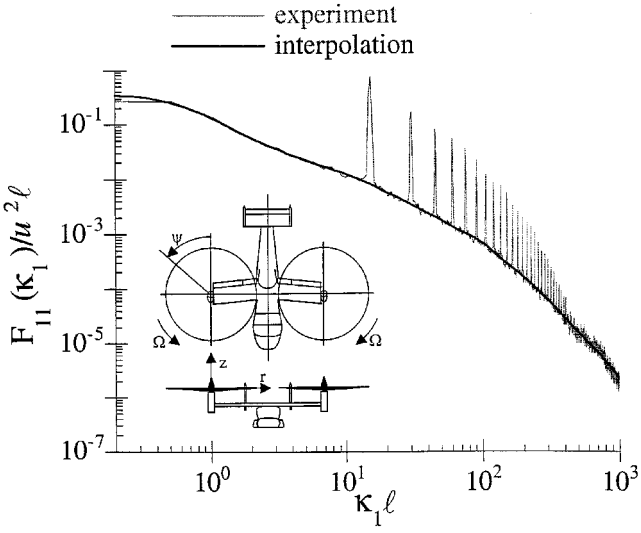

Fig. 2 Sample longitudinal spectrum and interpolated broadband part of the spectrum, at r/R = 0.917, ψ = 270 deg, and z/R = 0.083 above the rotor plane of the tiltrotor configuration.

Table 1 Scaling analysis

Quantity	Full-scale XV-15	Cornell model
Characteristic scales		
b	3	2
R, m	3.81	0.305
c_{tip}, m	0.152	0.019
C, m	1.60	0.13
w, m/s	17	6.88
V_{tip}, m/s	230	110
f_{tip}, Hz	29	115
Dimensionless parameters		
M_{tip}	0.67	0.32
Re_{tip}	2.3×10^6	1.4×10^5
Re_{in}	3.6×10^6	1.2×10^5
s/R	0.154	0.196
σ	0.103	0.074
Scaling factors		
ℓ_f/ℓ_m	12.5	
u_f/u_m	2.47	
p_f/p_m	Eq. (10)	

third of the rotor blades during the acoustic experiments. The lower Re_{tip} on the model probably caused the tip vortices generated by the model rotors to have a larger nondimensional core size, which could not be corrected. Finally, Re_{in} being smaller than full scale was not expected to affect the already turbulent mean flows or large-scale turbulence structures, which are a dominant characteristic of the fountain flow. The most significant consequence of the model Re_{in} being too low was a relatively coarse turbulence structure[30]: $\eta/\ell \propto (Re_{in})^{-3/4}$. However, the high wave-number turbulence is not important to the most annoying noise radiation, and this nearly isotropic part of the spectrum could easily be corrected by extending the Kolmogorov range to the full-scale microscale, $1/\eta_f$.

The wake vortex spacing was modeled reasonably well in the experiment. Matching s/R was important because the fountain flow is believed to be strongly influenced by this additional vorticity. With a semispan model, Swanson and Light[20] showed that remnants of the tip vortices seem to be transported by the fountain-flow backup between the rotor disk and the image plane. Similar results were found recently from the present model during experiments to evaluate semispan tiltrotor models. In those tests, the tip vortices were rapidly diffused above the rotor disk, ceased to follow repeatable paths, and their energy was cascaded into the turbulence of the fountain flow.[34] Thus, correctly simulating the turbulence energy injection rate by the tip vortices was more important than scaling the exact size or structure of the vortices.

Experimental Results and Discussion

The important results from the flow and noise measurements are described in the following sections, and comparisons are made with other experiments wherever possible. The effects of the diagonal fence are also described.

Flow Visualization

Figure 3 shows sample flow visualization from the tiltrotor configuration of the model. The camera was positioned at the rotor plane altitude, and helium bubbles were injected into the flow at the base of the fountain flow. Although symmetric in Fig. 3, the fountain flow randomly shifted from side to side across the longitudinal plane of symmetry of the model, and so it was often asymmetrically ingested by one rotor or the other. The time scale of this motion was on the order of seconds. This shifting of the fountain is a characteristic feature of this flow, and is important for interpreting the turbulence measurements described next. Further flow visualization studies were presented by Coffen et al.[19] and Polak and George.[32]

Hot-Wire Measurements

Figure 4 presents mean velocity vectors at $\psi = 270$ deg, $z/R = 0.083$ above the rotor plane, for 1) a single isolated rotor, 2) two rotors with no fuselage, and 3) complete tiltrotor configuration (see Fig. 2 for coordinate system). At most stations, the mean velocity component perpendicular to the page was zero (no mean azimuthal component); the exception was between the rotors of the tiltrotor configuration, where there was a mean flow toward the tail of the model caused by the direction of rotation of the rotors.

Comparing the isolated rotor with the two rotors with no fuselage reveals an interesting phenomenon. The presence of the second rotor without the aircraft fuselage substantially changed the flowfield near $\psi = 270$ deg. Although the magnitudes of the velocity vectors were about the same, their angles were different because of the different boundary conditions: the single rotor induced inflow from a symmetric and essentially infinite volume of fluid, whereas the available inflow volume for the two rotors without the fuselage was only semi-infinite for each rotor, and asymmetric. However, at $\psi = 90$ deg, the flowfields of both the two rotors without the fuselage and the tiltrotor configuration were the same as the isolated rotor. For nonoverlapping rotors, simple momentum theory predicts that there should be no rotor–rotor interaction.[35] However, experimental measurements of this configuration are conflicting: Dingeldein[36] found a 15% power reduction (lower

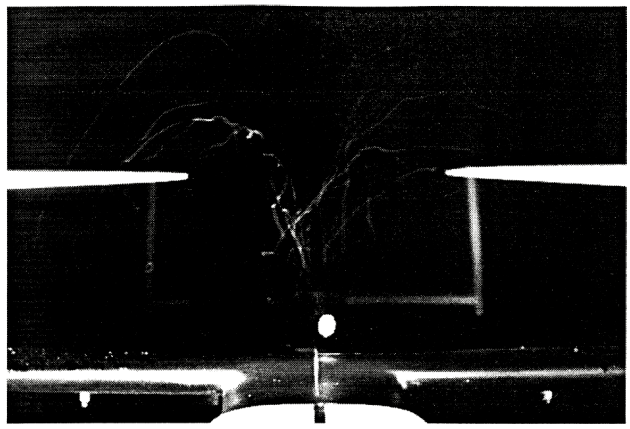

Fig. 3 Helium bubble flow visualization from the tiltrotor configuration.

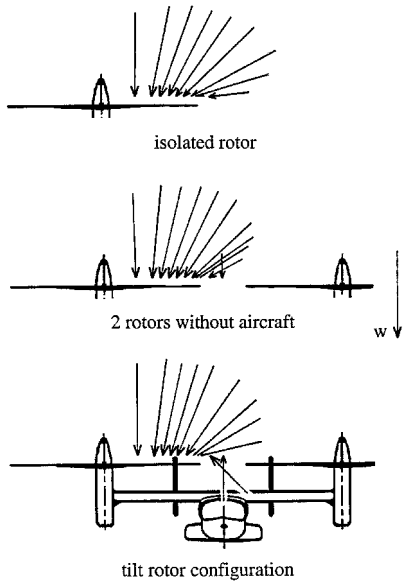

Fig. 4 Mean velocity vectors at $\psi = 270$ deg, $z/R = 0.083$ above the rotor plane.

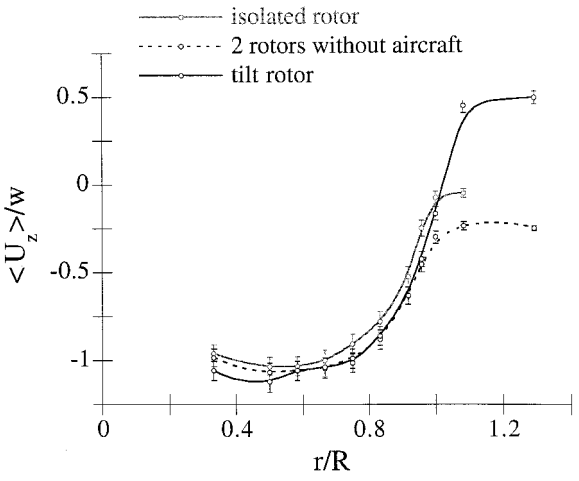

Fig. 5 Normalized mean inflow velocity at ψ = 270 deg, z/R = 0.083 above the rotor plane.

induced velocities), Sweet[37] found no significant difference, whereas Stepniewski and Keys[38] measured higher induced velocities.

Figure 5 plots the normalized inflow velocity component, $\langle U_z \rangle / w$, for the same three cases shown in Fig. 4, at ψ = 270 deg, z/R = 0.083 above the rotor plane. Smooth curves were drawn through the data points. The largest difference among the three cases occurred for $r/R > 1.0$: the tiltrotor configuration had positive $\langle U_z \rangle$ from the fountain flow, the two rotors with no aircraft had negative $\langle U_z \rangle$, and the isolated rotor had $\langle U_z \rangle$ nearly zero. Particularly in the acoustically important tip region, the inflow for the tiltrotor and two rotors without the fuselage was higher than the isolated rotor, so that blade angle of attack and blade loading were reduced. The magnitude of this rotor–rotor aerodynamic interaction was estimated from the measurements at z/R = 0.083, ψ = 270 deg, and predicted inflow velocities in the plane of the isolated rotor itself, $\langle U_z \rangle_{z=0}$. A hover prediction code using Prandtl's vortex theory[39] was used to estimate $\langle U_z \rangle_{z=0}$. This code contains empirical models for the effects of Reynolds number, Mach number, and blade element stall. To test the code, the measurements of Leishman et al.[40] were used. The overall thrust and the inflow velocity distribution in the rotor plane predicted by the code were in good agreement with the experimental data.[26]

Table 2 shows that, on the average, the rotor blades of both the tiltrotor and two rotors without the fuselage experienced a decreased effective angle of attack at ψ = 270 deg. Because the changes in angle of attack were small, the effect on overall rotor thrust was probably small (not measured). However, if the angle-of-attack changes occurred over a short azimuthal extent, the effect on harmonic noise would be substantial. Such a rotor noise source would be preferentially radiated behind the model, because of the direction of rotation of the rotors (from wing leading edge to trailing edge, as they sweep over the main wings), and Doppler amplification. In a large-scale experiment, Felker and Light[10] found a 1.6% reduction in rotor thrust when comparing their rotor plus image plane with their rotor alone, suggesting a reduced blade loading near the image plane. Also, Mosher and Light[22] found an increase of about 3–5 dB when comparing their rotor plus image plane case with their rotor alone. The noise increase was not simply a sound intensity increase caused by hemispherical vs spherical spreading. Instead, the image plane changed the inflow to the rotor, creating a disturbance that radiated as an impulse in the waveform. Moving the rotor 0.16R farther away from the image plane did reduce noise by about 2 dB. If the image planes in both Felker and Light's and Mosher and Light's experiments correctly simulated the aerodynamic presence of the second rotor, then both of these large-scale results are consistent with the present experiment, and they are important because they

Table 2 Angle-of-attack changes at ψ = 270 deg

r/R	Two rotors, no fuselage, deg	Tiltrotor configuration, deg
1.00	−0.82	−0.33
0.96	−0.77	−0.66
0.92	−0.41	−0.41
0.83	−0.43	−0.34

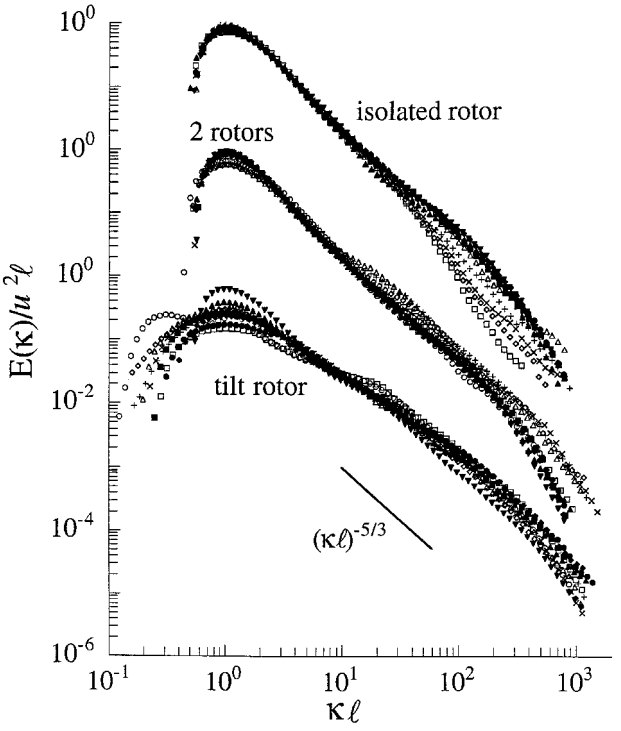

Fig. 6 Normalized turbulence spectra at ψ = 270 deg, z/R = 0.083 above the rotor plane: , r/R = 0.333; , r/R = 0.500; ♦, r/R = 0.583; ■, r/R = 0.667; ●, r/R = 0.750; △, r/R = 0.833; +, r/R = 0.917; ×, r/R = 0.958; ◇, r/R = 1.000; □, r/R = 1.083; and ○, r/R = 1.292.

prove that there can be a rotor–rotor interaction in hover, even between two rotors without the fuselage.

Figure 6 shows nondimensional turbulence spectra, $E(\kappa)/u^2\ell$, at several radial stations for the three configurations at ψ = 270 deg, z/R = 0.083 above the rotor plane. The spectra were found from the measurements using Eq. (6), and truncated at $\kappa = 1/\eta$. For the isolated rotor, the spectra at all radial stations collapsed well for $\kappa\ell < 200$, and exhibited Kolmogorov inertial subrange scaling: $E(\kappa) \propto (\kappa\ell)^{-5/3}$. Not surprisingly, the spectra diverged at the small scales because Re_ℓ varied from 3.3 × 10^3 at r/R = 1.083 to about 10^4 at $r/R < 0.5$, and $\eta/\ell \propto (Re_\ell)^{-3/4}$. Similar results were found for the two rotors with no fuselage, where Re_ℓ ranged from 5.5 × 10^3 at r/R = 1.292 to 2.4 × 10^4 at r/R = 0.958. The scatter among the spectra for different radial stations was largest for the tiltrotor configuration, even though Re_ℓ varied the least for this case: 10^4 at r/R = 1.292 to 2.1 × 10^4 at r/R = 0.750. Also, the decay of energy with wave number for the tiltrotor was less than predicted by the Kolmogorov spectrum model: $(\kappa\ell)^{-1.29}$ vs $(\kappa\ell)^{-1.67}$.

For the two stations located between the rotors of the tiltrotor configuration, r/R = 1.083 and r/R = 1.292, there were broadband peaks in the spectra at about $\kappa\ell$ = 20, corresponding to length scales in the flow of about 5 mm. This length is about $c_{tip}/4$, a reasonable estimate for the tip vortex cores. Considering the present flow visualization experiments, and the tip vortex trajectory measurements of Swanson and Light[20] and Polak et al.[34] described previously, this increased turbulence

energy near $\kappa\ell = 20$ was most likely caused by remnants of tip vortex cores convected by the mean flow backup between the rotors. This inflow of energy into the turbulence at a second length scale probably explains the slower decay of energy with wave number than that predicted by the Kolmogorov spectrum model.

The differences in the large scales of the turbulence spectra for the tiltrotor configuration were most likely caused by different inflow conditions over the rotor disk. Vortex stretching and tilting by the mean flow can change the frequency distribution and intensity of the turbulence, as discussed by Simonich et al.[41] Away from the fountain flow (near the rotor hub), fluid was induced into the rotor from a large distance away, and the flow underwent a large contraction. The strain rate associated with the flow contraction caused vortex stretching in the streamwise direction, and amplified velocity fluctuations in the n and b directions perpendicular to the streamwise direction. Thus, initially isotropic ambient turbulence was distorted by the potential rotor inflow, and became anisotropic by the time it arrived at the rotor disk, with increased energy in the cross-stream directions at the large scales. Support for this explanation is given in Fig. 7, which shows measured $F_{22}(\kappa_1)/u^2\ell$ for the tiltrotor configuration, compared with a theoretical relation for $F_{22}(\kappa_1)$ deduced from the measured $F_{11}(\kappa_1)$[42]:

$$F_{22th}(\kappa_1) = \left[F_{11}(\kappa_1) - \kappa_1 \frac{dF_{11}(\kappa_1)}{d\kappa_1} \right] \Big/ 2 \qquad (11)$$

Equation (11) is valid for isotropic, homogeneous turbulence, so that differences between the measured and theoretical $F_{22}(\kappa_1)$ indicate that the turbulence is anisotropic and/or nonhomogeneous. Van Atta and Chen[29] used the same procedure to detect isotropic turbulence. At $r/R = 0.333$, Fig. 7 shows that the experimental $F_{22}(\kappa_1)$ had significantly more energy than one would expect from Eq. (11) for $\kappa_1\ell < 40$. However, at higher wave numbers, the turbulence was closer to isotropic and homogeneous, judging by the better agreement between the measured $F_{22}(\kappa_1)$ and Eq. (11).

On the other hand, for regions of the flowfield in the fountain flow, the fluid followed a shorter path from the rotor wake back around through the rotor again, and did not experience the large flow contraction, so that one would assume this turbulence may be closer to isotropic. Figure 7 also shows the measured $F_{22}(\kappa_1)/u^2\ell$ at $r/R = 1.000$ for the tiltrotor configuration compared with Eq. (11). This time, the agreement between experiment and Eq. (11) is better at all wave numbers, indicating that this turbulence is indeed closer to isotropic.

For the stations in the range $0.5 \leq r/R \leq 0.9$, there was a gradual shift between nonfountain and fountain turbulence. More precisely, because of the time averaging used to generate the data shown in Fig. 6, the spectra in this intermediate region reflect the fraction of time that the fountain flow was present. Because of the shifting of the fountain flow across the longitudinal plane, described previously in the Flow Visualization section, a given blade element encounters either ambient turbulence, or the statistically very different fountain-flow turbulence, depending on the instantaneous position of the fountain.

Figures 8 and 9 plot the normalized velocity and length scales of the inflow turbulence computed from Eqs. (7) and (8). Results for the diagonal fences are also shown, which will be discussed in a later section. For the isolated rotor and two rotors with no fuselage, the turbulence over most of the rotor disk was characterized by relatively small velocity scales: $u/w \approx 0.04$, and large length scales: $\ell/R \approx 1.6$. Similar results were found for $r/R < 0.5$ of the tiltrotor configuration. These measurements corresponded to ambient room turbulence ingestion. However, in the fountain flow of the tiltrotor configuration, the turbulence was characterized by larger velocity scales and smaller length scales. In particular, ℓ/R in the fountain-flow region roughly matched $h/R = 0.39$, so that the fountain turbulence seemed to take its length scale from the rotor disk-to-wing clearance. In the intermediate region of the tiltrotor configuration, approximately $0.5 \leq r/R \leq 0.9$, the fountain-flow intermittency was evident because the plots of u/w and ℓ/R reflect the fraction of time that the fountain flow was present.

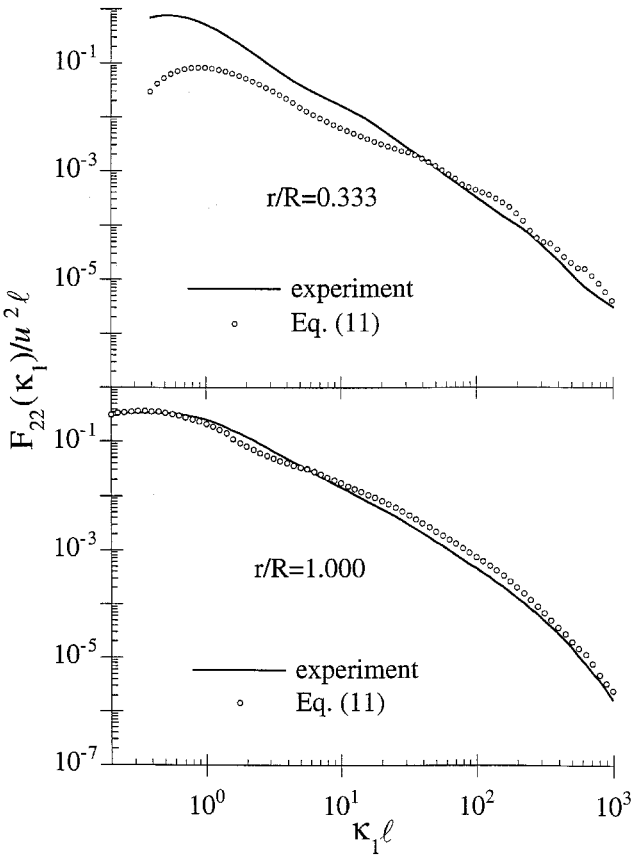

Fig. 7 Experimental and theoretical normalized transverse spectra at $\psi = 270$ deg, $z/R = 0.083$ above the rotor plane of the tiltrotor configuration.

Acoustic Measurements

Acoustic experiments were conducted on the same three configurations discussed previously. Using the approximate

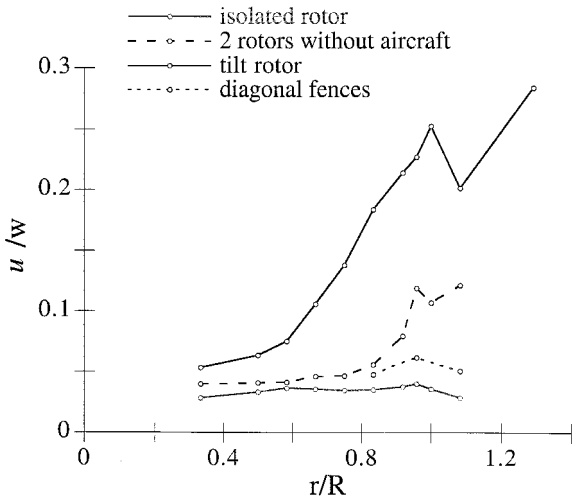

Fig. 8 Normalized turbulence velocity scales at $\psi = 270$ deg, $z/R = 0.083$ above the rotor plane.

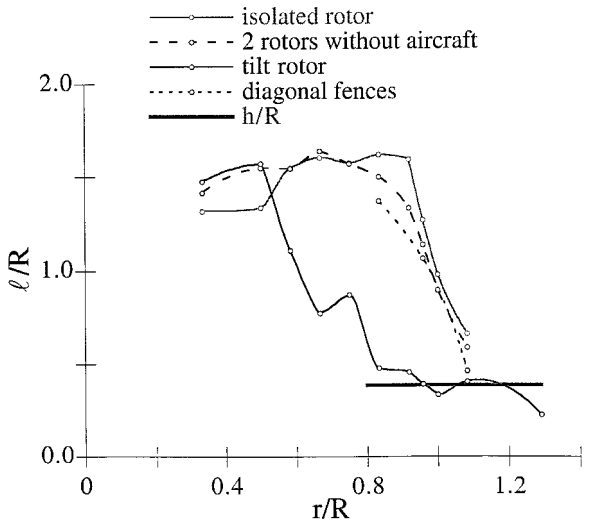

Fig. 9 Normalized turbulence length scales at ψ = 270 deg, z/R = 0.083 above the rotor plane.

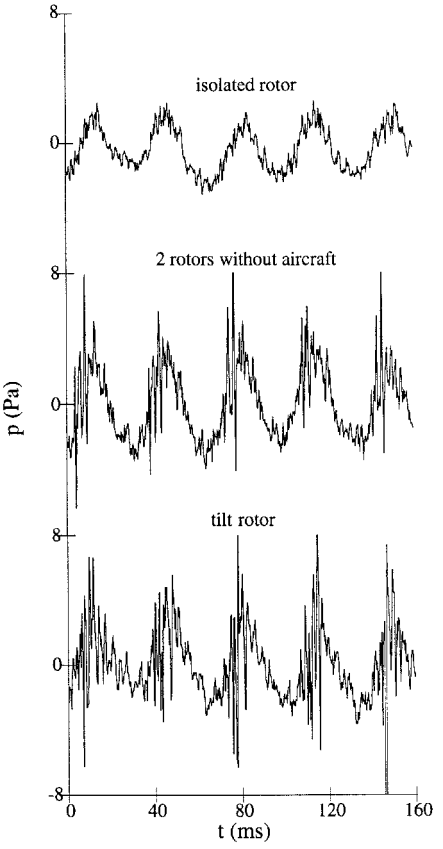

Fig. 10 Equivalent full-scale acoustic waveforms directly behind the aircraft, ρ = 218 m, 18.1 deg below the rotor plane.

scaling relation of Eq. (10), all data reported in this section have been extrapolated to the full-scale XV-15, at ρ = 218 m, to match the data of Conner and Wellman.[18]

Sample acoustic waveforms measured directly behind the model, 18.1 deg below the rotor plane, are shown in Fig. 10. As expected, the lowest amplitudes were found for the isolated rotor. Adding a second rotor increased the constant loading, Gutin noise amplitude,[43] but also added an impulsive part to the acoustic waveform. This impulsive part was much larger behind the model, and was more severe for larger angles below the rotor plane, suggesting that it was caused by a change in blade loading in the region between the rotors. This change in blade loading was not caused by a ground-based fountain flow, because the measured turbulence length scales were much smaller than the rotor plane altitude above the ground (0.5R to 1.5R vs 5.2R). Tuft flow visualization also confirmed that there was no ground-based fountain flow between the rotors. Instead, the change in blade loading was caused by the rotor–rotor interaction near ψ = 270 deg, as shown in Figs. 4 and 5. This rotor–rotor interaction had not been previously recognized as an acoustic source.

For the tiltrotor configuration, an impulsive part was also found in the waveforms. Once again, it was much larger behind the model, and was more severe for larger angles below the rotor plane, just as that found on the full-scale XV-15.[18] It should be emphasized that the mean and turbulent flowfields depicted in Figs. 4, 5, and 6 were the result of many ensemble averages, and any instantaneous realization of the flow could have been significantly different, as suggested by the unsteady acoustic waveforms of Fig. 10. The impulsive part of the waveforms seemed to vary on the order of a few seconds: sometimes it was mostly a positive pressure peak, other times it was mostly a negative pressure peak, and sometimes it was completely absent. Mosher and Light[22] also reported amplitude variations in the impulsive part of the acoustic waveforms measured behind their semispan tiltrotor model, and so did George et al.[4] on the XV-15. The impulsive part of the waveforms was probably caused by a superposition of rotor–rotor interactions (similar to those for the two rotors without the fuselage), rotor–fountain flow interactions, and possibly discrete interactions between the rotor blades and vortex filaments convected above the rotor plane by the fountain flow. Also, the observed unsteadiness in the acoustic waveforms was probably caused by the unsteadiness of the fountain flow itself.

Equivalent full-scale acoustic spectra for the same three cases are shown in Fig. 11. These plots further demonstrate that adding a second rotor in close proximity to an isolated

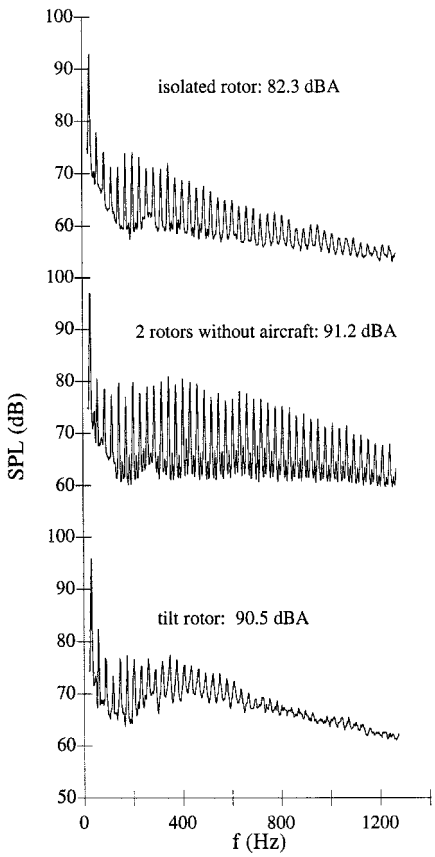

Fig. 11 Equivalent full-scale acoustic spectra directly behind the aircraft, ρ = 218 m, 18.1 deg below the rotor plane.

rotor increases the harmonic noise behind the rotors significantly. After A-weighting, the second rotor without the aircraft increased the noise radiation to 91.2 equivalent full-scale dBA, compared with 82.3 dBA for the isolated rotor. Significantly, at the same angle and distance in front of the two rotors with no fuselage, the sound pressure level was only 87.7 dBA. The extra 3.5 dBA behind the two rotors without the fuselage was a result of the impulsive acoustic source caused by the rotor–rotor interaction. Because of the direction of the blade motion, this source was preferentially radiated behind the rotors.

For the tiltrotor configuration, the presence of the wing and fuselage reduced the harmonic noise compared with the two rotors without the fuselage, but increased the broadband noise substantially. The reduced harmonic loading noise was expected, considering the smaller angle-of-attack changes at ψ = 270 deg, shown previously in Table 2. Also, the higher broadband noise for the tiltrotor configuration was expected because of the higher turbulence velocity scales and smaller turbulence length scales in the fountain flow, shown in Figs. 8 and 9. At the same angle and distance in front of the tiltrotor case, the measured sound pressure level was 87.5 dBA; about the same as the 87.7 dBA in front of the two rotors without the aircraft. Finally, before A-weighting, the overall sound pressure level for the tiltrotor was 99.2 dB directly behind the aircraft, which compares well with the full-scale data of Conner and Wellman,[18] who measured 96.9 dB at the same ρ and 12.6 deg below the rotor plane.

Effects of Diagonal Fences

The inset of Fig. 12 shows diagonal fences mounted on the model wings, which were designed to block the transport of blade wake and tip vorticity by the mean flow backup between the rotor disks, and reduce the radiated broadband noise. The inflow turbulence intensity, $u/\langle U \rangle$, in the tip region was reduced by a factor of about 3 by the diagonal fences. Also, the turbulence had a larger length scale, and smaller velocity scale, similar to the isolated rotor and two rotors without the aircraft, shown previously in Figs. 8 and 9. The fences were believed to be successful because flow visualization showed that the tip vortices were trapped on the hub side of the fences, and could not be recirculated by the mean flow.

Consistent with the reduced turbulence levels, broadband noise was also reduced by the diagonal fences, as shown in the acoustic spectra of Fig. 12, which were extrapolated to the full-scale from the model measurements using Eq. (10). The diagonal fences caused an equivalent full-scale noise reduction of about 4.1 dBA behind the aircraft. At the same angle and distance in front of the model with diagonal fences, the sound pressure level was 86.3 dBA; about the same as the 87.5 dBA of the tiltrotor configuration at the same observer location. Because most of the rotor noise from turbulence interactions in the fountain flow is propagated behind the model, reducing the extent of these interactions would not be expected to reduce acoustic emissions much in front of the model. The diagonal fences removed the well-known directionality of hovering tiltrotors, i.e., the radiated noise was the same behind the model as it was in front of the model.

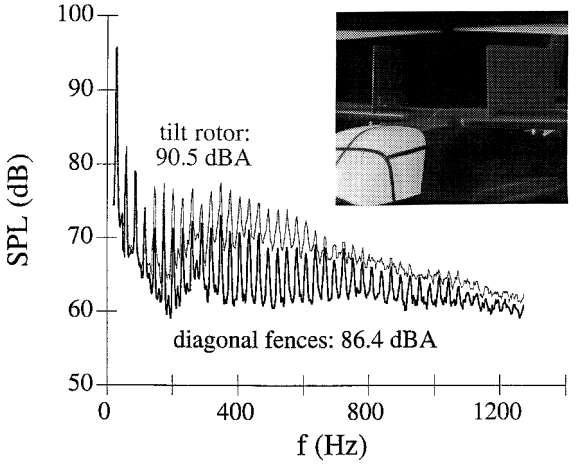

Fig. 12 Effect of diagonal fences on equivalent full-scale acoustic spectra directly behind the aircraft, ρ = 218 m, 18.1 deg below the rotor plane.

Conclusions

Rotor inflow aerodynamics and acoustic measurements were made on three configurations of an 8% scale model of the XV-15 tiltrotor in hover: 1) single isolated rotor, 2) two rotors with no fuselage, and 3) complete tiltrotor configuration. Scaling relations were given to extrapolate the model measurements to the full-scale aircraft. The principal conclusions of this research were as follows.

1) The impulsive noise of the tiltrotor configuration was caused by a superposition of rotor–rotor interactions, rotor–fountain-flow interactions, and possibly the discrete interactions between the rotor blades and vortex filaments convected above the rotor plane by the fountain flow. The observed unsteadiness in the acoustic waveforms was caused by the unsteadiness of the fountain flow itself.

2) The rotor–rotor interaction caused higher mean inflow velocity, and reduced blade loading at ψ = 270 deg for the tiltrotor and two rotors without the fuselage. This azimuthally varying blade loading increased harmonic loading noise behind the model. The two rotors without the fuselage radiated more harmonic loading noise than the tiltrotor configuration, consistent with the inflow measurements that showed that the tiltrotor had smaller mean angle-of-attack changes at ψ = 270 deg. This rotor–rotor interaction had not been previously recognized as an acoustic source.

3) The tiltrotor configuration radiated more broadband noise than two rotors with no fuselage. This acoustic result was consistent with the hot-wire experiments, which showed that the tiltrotor configuration had higher turbulence intensities at ψ = 270 deg.

4) The fountain turbulence had a higher velocity scale, smaller length scale, and was closer to isotropic than the ingested ambient turbulence. The fountain turbulence seemed to obtain its length scale from the rotor disk-to-wing clearance. Because of the constant positional shifting of the fountain flow, the inflow into the rotors was intermittent, alternating between ambient turbulence ingestion and fountain-flow turbulence ingestion. In the fountain flow, there was an inflow of energy into the turbulence at a second length scale that seemed to match the tip vortex core size ($c_{tip}/4$), and most likely explains the slower decay of energy with wave number than predicted by the Kolmogorov spectrum model: $(\kappa\ell)^{-1.29}$ vs $(\kappa\ell)^{-1.67}$.

5) Diagonal fences reduced the turbulence intensity in the fountain region by a factor of about 3, and reduced noise by 4.1 dBA behind the model. The fences were believed to be successful because the tip vortices were trapped on the hub side of the fences, and could not be recirculated by the mean flow. The diagonal fences removed the well-known acoustic directionality of hovering tiltrotors, because the radiated noise was the same behind the model as it was in front of the model.

Acknowledgments

This research was supported by NASA Ames Research Center Grant NAG-2-554. The authors would like to acknowledge Graduate Research Assistant Christian Bisogni, and Undergraduate Research Assistant John-David Bamford. Marianne Mosher is acknowledged for suggesting the diagonal fences.

References

[1]Albers, J. A., and Zuk, J., "Civil Applications of High Speed Rotorcraft and Powered Lift Aircraft Configurations," *Proceedings of*

the International Powered Lift Conference & Exposition (Santa Clara, CA), Society of Automotive Engineers, Warrendale, PA, 1987, pp. 627–651.

[2]Huston, R. J., Golub, R. A., and Yu, J. C., "Noise Considerations for Tiltrotor," AIAA Paper 89-2359, July 1989.

[3]McVeigh, M. A., "The V-22 Tiltrotor Large-Scale Rotor Performance/Wing Download Test and Comparison with Theory," *Proceedings of the 11th European Rotorcraft Forum* (London, England, UK), National Aerospace Lab., Emmeloord, The Netherlands, 1985.

[4]George, A. R., Smith, C. A., Maisel, M. D., and Brieger, J. T., "Tiltrotor Aircraft Aeroacoustics," *Proceedings of the 45th Annual Forum & Technology Display of the American Helicopter Society* (Boston, MA), American Helicopter Society, Alexandria, VA, 1989.

[5]Clark, D. R., "Analysis of the Wing/Rotor and Rotor/Rotor Interactions Present in Tilt-Rotor Aircraft," *Vertica*, Vol. 11, No. 4, 1987, pp. 731–749.

[6]Fejtek, I., and Roberts, L., "Navier-Stokes Computation of Wing/Rotor Interaction for a Tiltrotor in Hover," *AIAA Journal*, Vol. 30, No. 11, 1992, pp. 2595–2603.

[7]Meakin, R. L., "Moving Body Overset Grid Methods for Complete Aircraft Tiltrotor Simulations," AIAA Paper 93-3350, July 1993.

[8]Tadghighi, H., Rajagopalan, G., and Burley, C., "Simulation of Tiltrotor Fountain Flow Field Effects Using a Finite Volume Technique—An Aero/Acoustic Study," *Proceedings of the 51st Annual Forum & Technology Display of the American Helicopter Society* (Fort Worth, TX), American Helicopter Society, Alexandria, VA, 1995, pp. 77–92.

[9]Narramore, J. C., Vadyak, J., and Shrewsbury, G., "Navier-Stokes Computations of the Full V-22 Configuration Using Massively Parallel Computers," *Proceedings of the 52nd Annual Forum & Technology Display of the American Helicopter Society* (Washington, DC), American Helicopter Society, Alexandria, VA, 1996, pp. 1500–1513.

[10]Felker, F. F., and Light, J. S., "Aerodynamic Interactions Between a Rotor and Wing in Hover," *Journal of the American Helicopter Society*, Vol. 32, No. 2, 1988, pp. 53–61.

[11]McVeigh, M. A., Grauer, W. K., and Paisley, D. J., "Rotor/Airframe Interactions on Tiltrotor Aircraft," *Journal of the American Helicopter Society*, Vol. 35, No. 2, 1990, pp. 43–51.

[12]Felker, F. F., "Wing Download Results from a Test of a 0.658-Scale V-22 Rotor and Wing," *Journal of the American Helicopter Society*, Vol. 37, No. 4, 1992, pp. 58–63.

[13]Lee, A., and Mosher, M., "An Acoustical Study of the XV-15 Tiltrotor Research Aircraft," *Proceedings of the AIAA 5th Aeroacoustics Conference* (Seattle, WA), AIAA, New York, 1979.

[14]Coffen, C. D., and George, A. R., "Analysis and Prediction of Tiltrotor Hover Noise," *Proceedings of the 46th Annual Forum & Technology Display of the American Helicopter Society* (Washington, DC), American Helicopter Society, Alexandria, VA, 1990.

[15]Rutledge, C. K., Coffen, C. D., and George, A. R., "A Comparative Analysis of XV-15 Tiltrotor Hover Test Data and WOPWOP Predictions Incorporating the Fountain Effect," *Proceedings of the American Helicopter Society Technical Specialist Meeting* (Valley Forge, PA), American Helicopter Society, Alexandria, VA, 1991.

[16]Hoad, D. R., Conner, D. A., and Rutledge, C. K., "Acoustic Flight Test Experience with the XV-15 Tiltrotor Aircraft with the Advanced Technology Blade (ATB)," *Proceedings of the DGLR/AIAA 14th Aeroacoustics Conference* (Aachen, Germany), Deutsche Gesellschaft für Luft- und Raumfahrt e.v., Bonn, Germany, 1992, pp. 134–151.

[17]Coffen, C. D., and George, A. R., "Tiltrotor Broadband Hover Aeroacoustics," *Journal of Fluids Engineering*, Vol. 115, No. 4, 1993, pp. 568–572.

[18]Conner, D. A., and Wellman, J. B., "Hover Acoustic Characteristics of the XV-15 with Advanced Technology Blades," *Journal of Aircraft*, Vol. 31, No. 4, 1994, pp. 737–744.

[19]Coffen, C. D., George, A. R., Hardinge, H., and Stevenson, R., "Flow Visualization and Flow Field Measurements of a 1/12 Scale Tiltrotor Aircraft in Hover," *Proceedings of the American Helicopter Society Technical Specialist Meeting* (Valley Forge, PA), American Helicopter Society, Alexandria, VA, 1991.

[20]Swanson, A. A., and Light, J. S., "Shadowgraph Flow Visualization of Isolated Tiltrotor and Rotor/Wing Wakes," *Proceedings of the 48th Annual Forum & Technology Display of the American Helicopter Society* (Washington, DC), American Helicopter Society, Alexandria, VA, 1992, pp. 1323–1344.

[21]Wood, T. L., and Peryea, M. A., "Reduction of Tiltrotor Download," *Proceedings of the 49th Annual Forum & Technology Display of the American Helicopter Society* (St. Louis, MO), American Helicopter Society, Alexandria, VA, 1993, pp. 1177–1191.

[22]Mosher, M., and Light, J. S., "Study of Noise on a Small-Scale Hovering Tiltrotor," *Journal of the American Helicopter Society*, Vol. 41, No. 2, 1996, pp. 27–36.

[23]Champagne, F. H., and Sleicher, C. A., "Turbulence Measurements with Inclined Hot Wires, Part 2. Hot Wire Response Equations," *Journal of Fluid Mechanics*, Vol. 28, Pt. 1, 1967, pp. 177–182.

[24]Tutu, N. K., and Chevray, R., "Cross-Wire Anemometry in High Intensity Turbulence," *Journal of Fluid Mechanics*, Vol. 71, Pt. 4, 1975, pp. 785–801.

[25]Kline, S. J., and McClintock, F. A., "Describing Uncertainties in Single-Sample Experiments," *Mechanical Engineering*, Vol. 75, No. 1, 1953, pp. 3–8.

[26]Polak, D. R., "Experimental and Computational Investigation of Tiltrotor Hover Aeroacoustics," Ph.D. Dissertation, Cornell Univ., Ithaca, NY, Aug. 1996.

[27]Piziali, R. A., and Felker, F. F., "Reduction of Unsteady Recirculation in Hovering Model Helicopter Rotor Testing," *Journal of the American Helicopter Society*, Jan. 1987, pp. 54–59.

[28]Hardin, J. C., "Introduction to Time Series Analysis," NASA RP1145, Nov. 1990.

[29]Van Atta, C. W., and Chen, W. Y., "Measurements of Spectral Energy Transfer in Grid Turbulence," *Journal of Fluid Mechanics*, Vol. 38, Pt. 4, 1969, pp. 743–763.

[30]Tennekes, H., and Lumley, J. L., *A First Course in Turbulence*, MIT Press, Cambridge, MA, 1972, pp. 20, 21.

[31]Alexander, H. R., Maisel, M. D., and Giulianetti, D. J., "The Development of Advanced Technology Blades for Tilt-Rotor Aircraft," *Vertica*, Vol. 10, No. 3/4, 1986, pp. 315–339.

[32]Polak, D. R., and George, A. R., "Experimental Aerodynamic and Aeroacoustic Investigation of a Scaled Tiltrotor in Hover," *Proceedings of the 50th Annual Forum & Technology Display of the American Helicopter Society* (Washington, DC), American Helicopter Society, Alexandria, VA, 1994, pp. 61–79.

[33]Farassat, F., and Succi, G.P., "The Prediction of Helicopter Rotor Discrete Frequency Noise," *Vertica*, Vol. 7, No. 4, 1983, pp. 309–320.

[34]Polak, D. R., Rehm, W., and George, A. R., "Effects of an Image Plane on Simulating a Model Tiltrotor in Hover," *Proceedings of the American Helicopter Society Technical Specialist Meeting* (Fairfield County, CT), American Helicopter Society, Alexandria, VA, 1995, pp. 66–78.

[35]Johnson, W., *Helicopter Theory*, Dover, New York, 1980, pp. 118–122.

[36]Dingeldein, R.C., "Wind-Tunnel Studies of the Performance of Multirotor Configurations," NACA TN 3236, Aug. 1954.

[37]Sweet, G. E., "Hovering Measurements for Twin-Rotor Configurations with and Without Overlap," NASA TN D-534, Nov. 1960.

[38]Stepniewski, W. Z., and Keys, C. N., *Rotary-Wing Aerodynamics*, Vol. 2, Dover, New York, 1984, p. 190.

[39]McCormick, B. W., *Aerodynamics of V/STOL Flight*, Academic, San Diego, CA, 1967, pp. 82–86.

[40]Leishman, J. G., Baker, A., and Coyne, A., "Measurements of Rotor Tip Vortices Using Three-Component Laser Doppler Velocimetry," *Proceedings of the American Helicopter Society Technical Specialist Meeting* (Fairfield County, CT), American Helicopter Society, Alexandria, VA, 1995, pp. 37–57.

[41]Simonich, J. C., Amiet, R. K., Schlinker, R. H., and Greitzer, E. M., "Rotor Noise Due to Atmospheric Turbulence Ingestion—Part I: Fluid Mechanics," *Journal of Aircraft*, Vol. 27, No. 1, 1990, pp. 7–14.

[42]Hinze, J. O., *Turbulence*, McGraw–Hill, New York, 1975, p. 204.

[43]Gutin, L. Y., "On the Sound Field of a Rotating Propeller," NACA TM-1195 (1948); translated from *Physikalische Zeitschrift der Sowjetunion*, 1936, pp. 57–71.